An Adhesive-Integrated Stretchable Silver-Silver Chloride Electrode Array for Unobtrusive Monitoring of Gastric Neuromuscular Activity

Jonas F. Kurniawan, Boris Tjhia, Vincent M. Wu, Andrew Shin, Nathan L. J. Sit, Timothy Pham, Andrew Nguyen, Carleen Li, Rajan Kumar, Marcelo Aguilar-Rivera, Imanuel Lerman, David C. Kunkel, and Todd P. Coleman*

Here, an unobtrusive, adhesive-integrated electrode array for continuous monitoring of stomach electric activity is introduced. This patient-friendly, disposable peel-and-stick adhesive device represents an important advancement over existing arrays that require placement of each electrode individually and are thus also labor intensive and are in general more rigid and cumbersome. In comparison to other silver–silver chloride electrodes, this skin conformal array does not require gel and thus can withstand low impedance over the duration of long recordings. Interfacing these electrodes with miniaturized electronic recording and wireless telemetry systems has the potential to enable scalable population health opportunities to perform objective gastrointestinal assessment and optimization of treatment regimens.

1. Introduction

Gastrointestinal (GI) problems are the second leading cause of missing school or work after the common cold.[1] The financial burden associated with GI problems is estimated to be $142B annually.[2] A majority of such cases are referred to GI specialists, where endoscopy, imaging, and blood tests readily allow for easy diagnosis of structural and inflammatory pathology, such as a blockage or infection. However, more than half of GI disorders involve an abnormal functioning of the GI tract, in the absence of any structural defect, and these types of disorders occur in a majority of Parkinson's and diabetes patients

for instance.[3,4] Diagnosis of such "functional" GI disorders typically entails subjective symptom-based questionnaires or objective but invasive procedures (e.g., gastric scintigraphy and manometry) in specialized centers. Symptom-based diagnosis is problematic because many GI functional disorders with different treatment regimens have overlapping symptoms. Most current clinically indicated objective approaches have drawbacks of cost and invasiveness. For instance, gastric involves radioactive imaging and manometry involves a catheter inserted through the mouth or nose with fluoroscopic or endoscopic guidance. With regards to disorders involving the foregut, motor aspects of stomach function do not correlate robustly with symptoms before or after treatment.[5–7] However, recent findings with invasive recordings show that electrical patterns of the stomach align well with disease diagnosis, symptoms, as well as treatment response.[8–12] As such, there is a unique opportunity to extract this spatial electrical information non-invasively.

GI smooth muscle contractions are governed by underlying rhythmic bio–electrical signals, known as slow waves, that are generated by oscillating pacemaker cells, the interstitial cells of Cajal. These slow waves have a frequency of 0.05 Hz in the stomach and underlie the electrogastrogram (EGG) signal that

J. F. Kurniawan
Materials Science and Engineering Program
University of California, San Diego
La Jolla, CA 92093, USA

J. F. Kurniawan, V. M. Wu, C. Li, Dr. M. Aguilar-Rivera, Prof. T. P. Coleman
Department of Bioengineering
University of California, San Diego
La Jolla, CA 92093, USA
E-mail: tpcoleman@eng.ucsd.edu

B. Tjhia, A. Shin, T. Pham, Dr. R. Kumar
Department of Nanoengineering
University of California, San Diego
La Jolla, CA 92093, USA

The ORCID identification number(s) for the author(s) of this article can be found under https://doi.org/10.1002/admt.202001229.

N. L. J. Sit
Department of Electrical and Computer Engineering
University of California, San Diego
La Jolla, CA 92093, USA

A. Nguyen
Department of Physics
University of California, San Diego
La Jolla, CA 92093, USA

I. Lerman
Department of Anesthesiology
University of California, San Diego
La Jolla, CA 92093, USA

D. C. Kunkel
GI Motility and Physiology Program
University of California, San Diego
La Jolla, CA 92093, USA

**ADVANCED
SCIENCE NEWS**
www.advancedsciencenews.com

**ADVANCED
MATERIALS
TECHNOLOGIES**
www.advmattechnol.de

can be recorded non-invasively with electrodes placed on the abdomen.[13]

Although it is non-invasive and easy to administer, conventional EGG suffers from limitations in interpretability and insufficient association with invasive clinical gold standards.[14,15] Recently, a large array of electrodes and statistical signal processing methodology, termed high-resolution electrogastrography (HR-EGG),[16] have been shown to detect gastric myoelectric dysfunction in common foregut disorders. Specifically, patterns from HR-EGG correlate with invasive measures[17] as well as symptom severity in patients with functional dyspepsia and gastroparesis.[18] It has also been shown that gastric slow wave parameters are distinct in healthy controls compared to patients with diabetic gastroparesis.[19] It was also recently shown that in children, spatiotemporal characterization of gastric slow wave activity using HR-EGG distinguishes symptomatic chronic nausea patients from healthy subjects.[20] Key opinion leaders have suggested that efforts be placed to confirm these findings in larger and more heterogeneous patient populations.[21]

Although findings from HR-EGG show great promise, all prior works relied on placing individual electrodes on the skin overlying the stomach with precise electrode interdistances.[16,18] Furthermore, commercial electrodes are pregelled, which means that during continuous long-term recording, electrodes may dry and change their electrode–skin impedance which can result in inaccuracy of the reading.

Herein, we present a single stretchable adhesive-integrated multi-electrode array that enables continuous unobtrusive monitoring of the EGG. This patient-friendly, disposable peel-and-stick adhesive embedded device completely eliminates the challenges associated with a previous generation wearable EGG monitoring system.[16–18] Further, silver-silver chloride (Ag/AgCl) as the electrode material of the sensor array alongside conformal contact with the human skin enables this class of flexible electronics to attain high signal-to-noise ratio (SNR) at the EGG frequency of 0.05 Hz.

Previously, this class of epidermal devices was successfully used to monitor fast-moving electrophysiologic signals, such as electroencepalogram (EEG), electrocardiogram (ECG) and electromyogram,[22–24] using gold as the component of the electrode in contact with skin. Those signals typically have spectral components at frequencies of 1 Hz above. However, at lower frequencies, such as 0.05 Hz associated with EGG, the polarizable nature of gold or metal electrodes in general, creates an offset potential at the electrode–skin junction that will interfere with the underlying slow electrophysiological signals of interest.

Since the signal of interest pertaining to EGG is 0.05 Hz, this implies that in this recording region, gold is very susceptible to DC noise. To elaborate, gold electrodes exhibit a high electrode–skin impedance, due to low ion mobility, which will form a barrier for the biopotential waveform to cross. On the flipside, Ag/AgCl electrodes are non-polarizable and allow for their Cl^- ion to partake in free charge exchange which eliminates charge buildup.[25,26] It has been established that for very slow frequencies (e.g., <1 Hz), Ag/AgCl exhibits very consistent and very low offset voltage, resistance, polarization, and drift, in comparison to variability in these parameters for gold and other metals.[25–27]

Fabrication of stretchable electronics is typically performed using equipment associated with standard complementary metal-oxide semiconductor (CMOS) processes, such as thin film deposition, dry etching, and photolithography.[22,24,28] However, the type of materials that can be deposited in a clean room setting is very limited, and excludes Ag/AgCl. One possible approach for fabricating stretchable Ag/AgCl electrode arrays involves post-clean room processes that include chlorination (e.g., dipping in ferric chloride ($FeCl_3$)) of exposed silver (Ag) film. However, performing this task with thin films that are sputter/electron beam-deposited present certain vulnerabilities to consistently produce low-impedance sensors that are mechanically robust. On the one hand, impedance decreases with thickness, but on the other hand, it is very challenging to produce a metal layer that is very thick (e.g., >1 µm) with a clean room deposition tool. The Ag film needs to be thick due to the chlorination process that converts most of the Ag into AgCl. In order for the sensor array to work as intended, a bilayer of Ag/AgCl is needed. Therefore, the film needs to be thick enough to leave the Ag component alongside the converted AgCl. AgCl film alone is very brittle, powdery, and has high impedance.

Further, the lack of process control in submerging a wafer with Ag film exposed in a chlorinated solution (e.g., $FeCl_3$) results in very low yield due to failure modes including film disintegration or electrodes with very high impedance (MΩ). Specifically, impedance of the AgCl layer depends on multiple factors, including thickness of Ag thin film deposited, the concentration of the $FeCl_3$ solution, as well as the amount of time that the Ag film is submerged inside the chlorinated solution. To elaborate more on the limitations, first, it is very challenging to produce an Ag layer that is very thick (e.g., >1 µm) with a clean room deposition tool. Second, the lack of process control pertaining to creation of the Ag/AgCl layer with the chlorination method often results in poor film quality (e.g., film becomes powdery and non-binding to the surface of the insulator beneath it). To be deemed usable, the Ag/AgCl film needs to be relatively uniform spatially, have a smooth surface, and have relatively low impedance. Given the limitation of depositing thick metal films with standard CMOS technology, it is sensible to explore printing methodologies to create reliable thick film layers for sensing applications.[29,30]

In this study, we successfully combine a hybrid approach that merges thin film CMOS processing technology and thick film screen printing technology[31,32] to demonstrate the first successful flexible dry Ag/AgCl electrode arrays for EGG monitoring. Marrying the two techniques results in a device that is easily embedded in adhesive, disposable, and easy to apply.

2. Results

Wafer-level fabrication was carried out using standard CMOS procedures as outlined in the Experimental Section. **Figure 1**c shows the cleanroom-produced silicon wafer containing the sensor array prior to the screen printing process of the Ag/AgCl layer. This wafer was then screen-printed with Ag/AgCl ink using a 75 µm thick standard stainless-steel stencil which yielded a 37.5 µm thick Ag/AgCl layer. The ink was solely printed on the active sensor area (ten circles of 8.6 mm diameter). The resulting device, including the Ag/AgCl layer, is shown in Figure 1d. Upon completion, the device was then transfer-printed using a water-soluble tape to a silicone (Ecoflex)/silicone adhesive (Silbione) substrate as shown in Figure 1e.
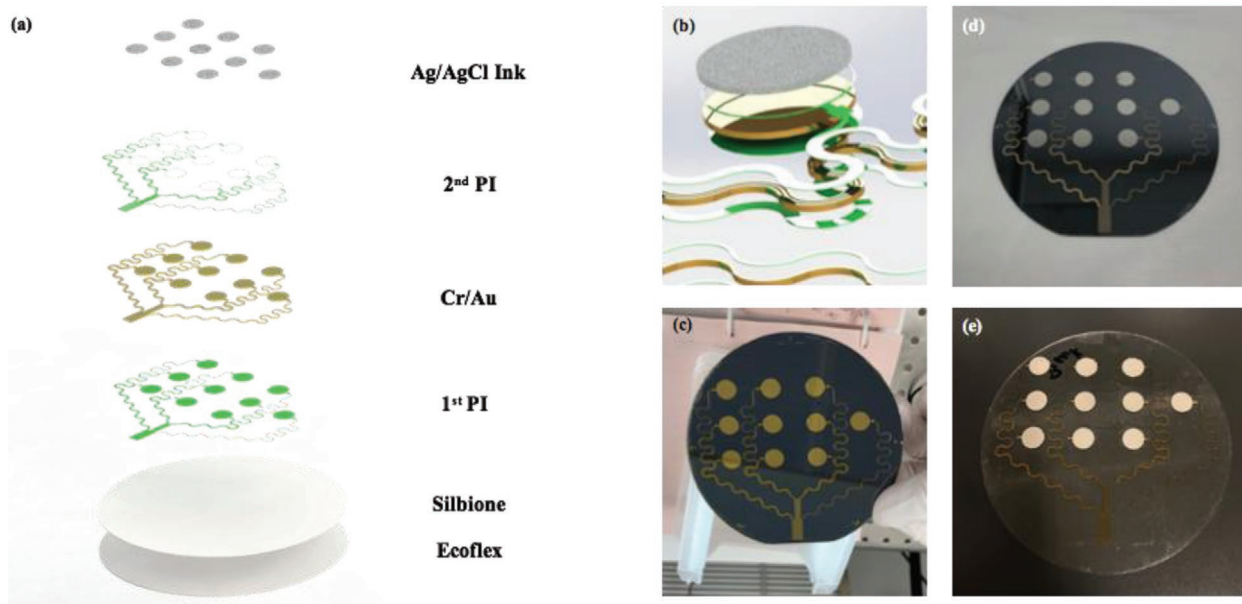
Figure 1. a) Cross section of the entire device (86 mm sensor diameter and 200 µm interconnect width). b) Close-up cross section of the sensor layer, consisting of the bottom PI layer, Au, PI mesh, and Ag/AgCl printed layer. c) Finished EGG device fabricated on a silicon wafer with Au on top layer before the screen printing process of Ag/AgCl has begun. d) EGG device screen-printed with Ag/AgCl ink on the active sensor area (37.5 µm). e) EGG device transferred into a flexible self-adhering silicone surface via water-soluble tape; the adhesive-integrated sensor array is now ready to be placed on the abdomen.

We implemented an electrical impedance spectroscopy (EIS) procedure to determine the impedance of our electrodes across different frequencies. We immersed the electrodes in a 0.9% NaCl (154 mM) solution (physiological concentration which is isotonic to body fluids) to simulate the physiologic properties of human body fluids.[33]

We ran EIS for three different types of electrodes, the standard 3M Red Dot that acted as a control, the Au flexible sensor (before screen-printed with Ag/AgCl), and the screen-printed Ag/AgCl flexible sensor. BioLogic SP-200 potentiostat (PEIS function) was used to sweep from 0.01 to 5 Hz and impedance was measured in units of Ω. Since a material's impedance is inversely proportional to its surface area, we compared different electrodes of different surface areas with the area specific impedance (ASI) which was in the unit of $\Omega \cdot mm^2$.[34]

It can be seen from **Figure 2**c that the general characteristic of decay in ASI with an increase in frequency is due in part to the inverse relationship between impedance and frequency in capacitive materials. It can be seen that the 3M Red Dot
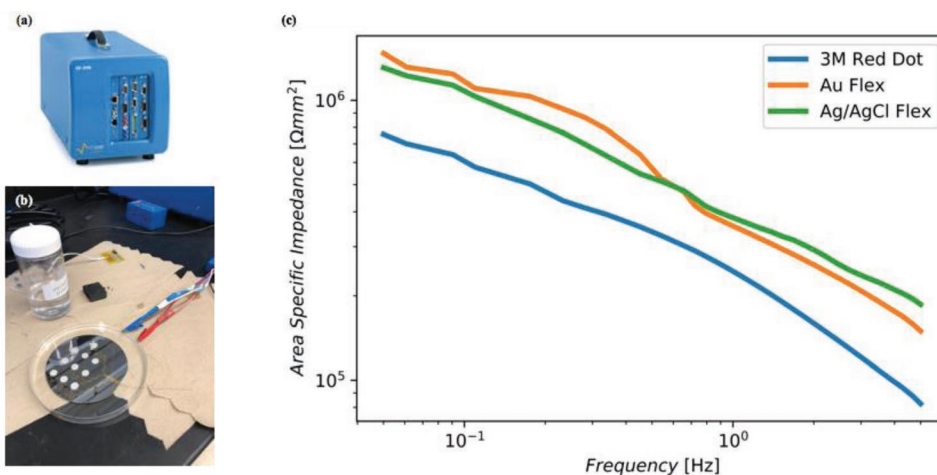

Figure 2. a) BioLogic SP-200 potentiostat used to gather measurements of electrochemical impedance spectroscopy (EIS). b) The sensor was connected to the positive (+) lead of the potentiostat; meanwhile, the negative (−) terminal of the potentiostat was connected to the NaCl solution via a metal header pin. The data were captured using PEIS function (potentiostatic EIS, where voltage is changed and current is measured). c) EIS data for multiple electrode types is shown. The graph displays area specific impedance (ASI) variation as frequency changes from 0.01 to 5 Hz for 3M Red Dot (commercial), Au flexible electrodes (before Ag/AgCl screen printing), as well as the Ag/AgCl flexible electrodes. The ASI of Ag/AgCl flexible electrodes is lower than that of Au flexible electrodes for frequencies between 0 and 0.6 Hz, which includes the EGG frequency of 0.05 Hz.
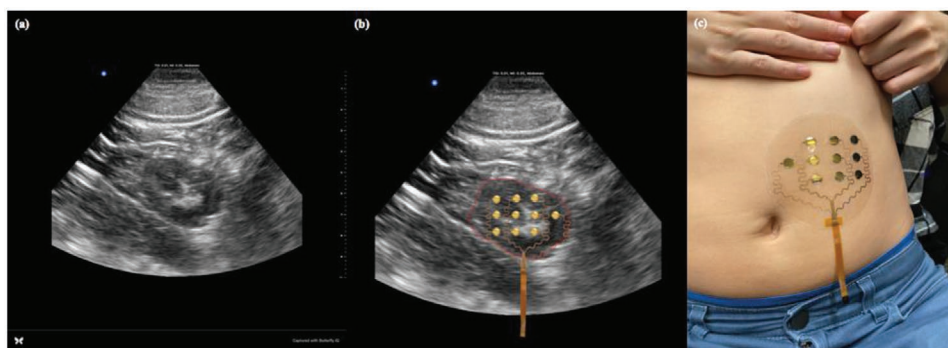
Figure 3. a) Coronal ultrasound image of the stomach location of one subject which was used to guide the placement of electrodes. b) Electrodes image was overlaid to the ultrasound image of stomach antrum to visualize the alignment of the electrode array to the stomach. These images were obtained using Butterfly IQ portable ultrasound system. c) Electrodes array was placed directly on top of the stomach location that was found previously using the ultrasound image.

electrode had the lowest ASI at every single frequency point compared to the flexible Au and flexible Ag/AgCl sensors. This behavior was expected due to the fact that 3M Red Dot is a wet electrode with conductive gel, as well as the fact that the Ag/AgCl was bulk in thickness (e.g., not thin film). However, for low frequency domain, specifically from 0.01 to 0.6 Hz, Ag/AgCl flexible electrodes showed lower ASI than Au flexible electrodes. This behavior is expected because of aforementioned resistance, polarization, and drift challenges at low frequencies associated with Au electrodes.[25,26] Usage of different classes of Ag/AgCl inks, with different ratios of particle ingredients, may allow for optimization to further reduce impedance.

Once EIS characterization was performed, we proceeded to place the electrode array on the abdomen for data collection. It has been established that there is high variability in interindividual stomach location relative to visible skin-based landmarks for electrode placement (e.g., the xiphoid and umbilicus).[18] Ultrasound is used to locate the antrum of the stomach for many purposes, including assessing gastric contents and volume.[35] Building upon this, we took advantage of a newly

developed portable ultrasound system that can be interfaced with a mobile phone/tablet to enable fully ambulatory image-guided placement of the electrodes array over the antrum. A representative result of the ultrasound image for one patient could be seen on **Figure 3**a.

Ultrasound images for test subjects were gathered to verify the placement of the electrodes. The Butterfly IQ portable ultrasound system was used to image the abdomen area of the subjects to locate the stomach location (setting: abdomen mode at 10 cm depth and 21–22 Hz frequency). Before imaging, the subject was asked to drink 8 oz of water, followed by the application of ultrasound gel to aid the imaging. Subjects were instructed to sit on a chair while leaning their backs against it. The ultrasound transducer probe was lightly pressed against the subject's abdomen and swept vertically to locate the stomach. Subjects were instructed to lie sideways to get a secondary scan to increase sensitivity of stomach localization. After stomach localization, the electrode array was placed over the antrum (Figure 3b).

One human subject's electrode array and recording analyses are shown in **Figure 4**. Filtered waveforms from electrodes
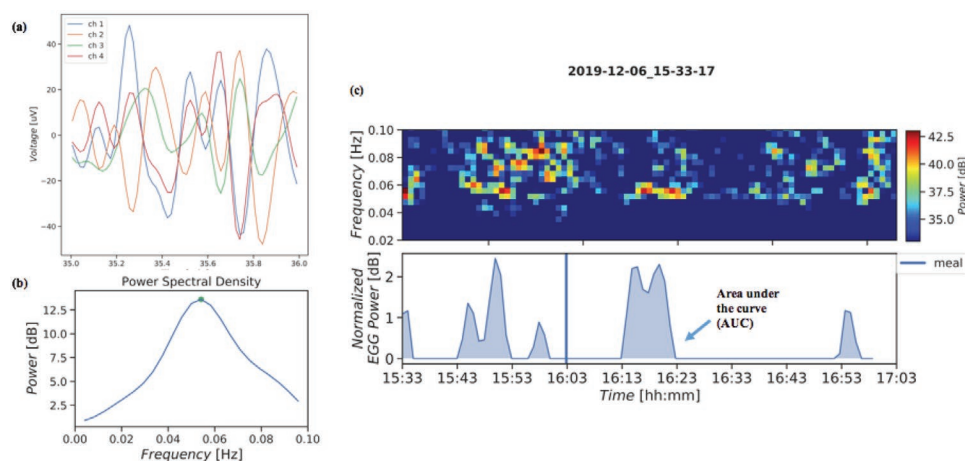

Figure 4. a) Recording data showing four out of the eight channels electrodes array. Slight shift of the signals is suggestive that the wave was propagating. Band pass filtering was done between 0.01 and 0.1 Hz to filter out ECG and other fast moving signals. b) Spectral representation of the signal from one electrode indicated a clear peak at 0.053 Hz. c) Spectrogram from one electrode indicated high energy around 0.05 Hz (indicative of EGG signals) that started around 3:43 PM (preprandial), 4:03 PM (meal), and 4:13 PM (postprandial). Large areas under the curve and red spectrogram were indicative of clear gastric signals.
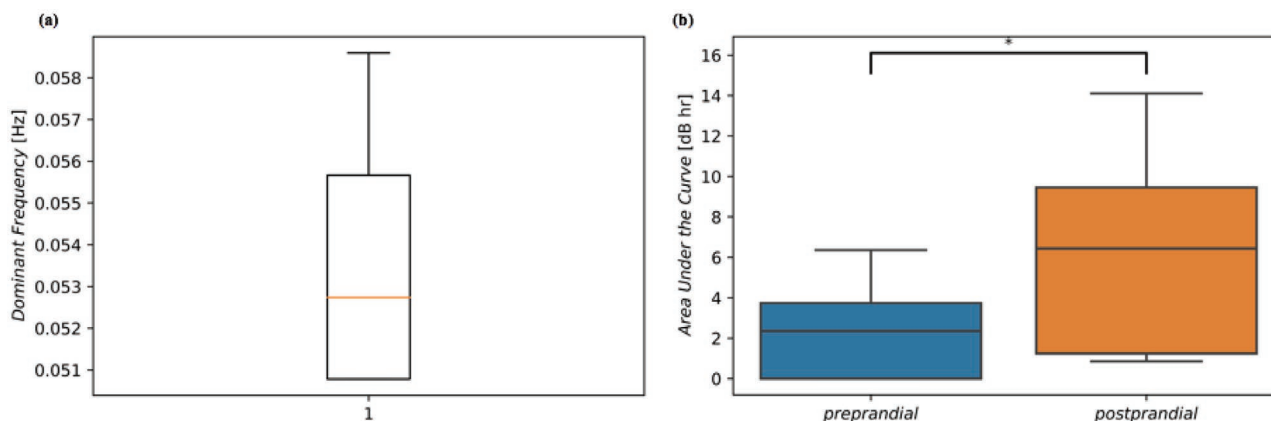
Figure 5. a) A box plot indicative of median peak in spectral power of 0.0527 Hz, and 25th to 75th interquartile range spanning from 0.051 to 0.0555 Hz. b) A box plot of area under the curve (AUC) for 30-min preprandial and postprandial intervals. A statistically significant increase from preprandial to postprandial AUC was found.

1 through 4 are shown in Figure 4a. After performing artifact rejection algorithms tailored to EGG recordings,[17] our methods as shown in Figure 4b represent a strong peak in the spectral representation of the processed signal at 0.053 Hz, near the gastric pacemaker frequency of 0.05 Hz that underlies the EGG. This spectrographic representation is comparatively superior to other findings of the literature that have prohibitive noise due to artifacts and other sources of noise.[36] The top of Figure 4c shows a spectrogram indicative of spectral power (in dB) at frequencies between 0 and 0.1 Hz across time. The bottom of Figure 4d shows normalized EGG (pertaining to the band of 0.03–0.07 Hz) which was defined as zero when below a statistically defined baseline (described in the Experimental Section). A large increase in normalized EGG power occurred and persisted ≈10 min after the subject had a meal. The area under the curve (AUC) of the normalized EGG power in the 30-min postprandial (e.g., after meal consumption) interval exceeded that of the 30-min preprandial (e.g., before meal consumption) interval.

Across all ten subjects, the median peak in spectral power was 0.053 Hz with a standard deviation of 0.004 Hz. Further, the difference between 30-min postprandial AUC and 30-min preprandial AUC was statistically significant (one-sided t-test, $p < 0.05$). These results are showcased in **Figure 5**.

3. Discussion

We have demonstrated an unobtrusive adhesive-integrated flexible and stretchable multi-electrode array for continuous and non-invasive measurement of the neuromuscular activity of the stomach manifested in the EGG. Furthermore, we addressed the problems associated with long-duration recordings with wet electrode systems through this new class of adhesive-integrated electrodes that utilizes a combination of lithography-based technique as well as screen printing of dry Ag/AgCl ink. We have successfully eliminated the challenge of limited materials selection associated with the ordinary lithography-based technique. In order to address intersubject variability in stomach location, we have shown that dependence on volumetric imaging at a facility (e.g., a CT or MRI scan) can be replaced with the use of a portable handheld ultrasound system, at the time of electrode placement, that can be interfaced with a mobile device.[18] This successful integration of using an ultrathin adhesive-integrated multi-electrode array, guided with mobile imaging, increases the plausibility that highly accurate fully ambulatory neuromuscular GI monitoring is feasible.

Our observation of all subjects having normal gastric activity within the range of 2–4 cycles/min is consistent with other EGG findings in normative controls following meal consumption.[37]

Patients with gastric disorders sometimes exhibit irregular neuromuscular activity that can include tachygastria (above 4 cycles/min) and bradygastria. (below 2 cycles/min)[38,39] The combination of our novel Ag/AgCl electrodes, which remove baseline drift, as well as the motion artifact rejection algorithm, which removes short bursts of high-amplitude activity, suggest that tachygastria can be captured with this approach. On the flipside, given that baseline drift is prone to occur during long-duration recordings, more evidence is needed to determine if this class of electrodes is robust to the detection of bradygastria for ambulatory recordings. Modern dynamic signal processing algorithms that utilize Bayesian inference, group sparsity, and multitaper methods may complement the optimization of future electrodes to yield further improvements.[40–42]

The statistically significant increase in AUC of the normalized EGG power from preprandial 30-min windows to postprandial 30-min windows across the group of ten subjects is consistent with findings associated with meal consumption. Specifically, we expected an increase in sustained normalized EGG power since ingestion of food is known to active excitatory neural responses of the stomach that increase the force of gastric smooth muscle contractions, and since the strength of gastric contractions is associated with the magnitude of EGG waveforms.[43–45] It is plausible that future studies that involve ambulatory EGG monitoring with this technology may use features such as the AUC or time duration until postprandial-normalized EGG power returns to baseline, to determine associations with symptom severity in patients with upper GI disorders.

A logical next step to evolve this technology is to perform 24-h recordings in normal subjects and patients with GI disorders

to understand the relationship between meals, EGG patterns, symptoms, and interventions such as medication(s). This is particularly relevant, as it is well known that GI symptoms are transient and sometimes do not occur during a clinic visit. Moreover, development of a non-invasive EGG system allows for evaluation of specialized patient populations such as neonates, children, older adults, and pregnant women, groups who often experience GI symptoms but are ineligible for invasive testing. Opportunities to match symptom logs by patients with patterns from EGG waveforms may allow for modern machine learning techniques to aid GI specialists in disambiguating the causes of symptoms and optimize treatment regimens. It was recently shown that 90-min recordings with 25 individual electrodes interfaced to a conventional bulky amplification system allow for the extraction of spatial patterns from the high-resolution EGG that correlate with symptom severity.[18]

While we have moved from a bulky wearable electronic device[17] to a flexible and stretchable electrode array, we have neither performed a 24 h recording with our electrode array nor recorded from a sufficient number of channels to extract spatial patterns. In such studies, it will be ideal to utilize miniaturized biopotential boards, such as the WAND Mini,[46] the BioADC board,[47] or the Intsy board[48] in an ambulatory study, in order to match the minimal invasiveness of the stretchable electrode array and record from 25 or more channel inputs to enable extracting spatial patterns. Since such an electrode array would be applied once to the skin and interfaced to a miniaturized board without long cables, significant noise reduction will ensue—further improving the ability to resolve spatial patterns.

The increasing attention being placed on slow electrical oscillations (<1 Hz) in the brain may allow for the use of these technologies in EEG recordings.[27,49,50] Further, recent efforts attempting to understand the electrophysiological interplay between the brain, autonomic nervous system, and stomach may allow for this class of sensors to be employed in joint EEG and EGG recordings.[51,52]

Wearable ECG technology has generated significant improvements in detection of events and informing diagnosis and treatment response for cardiovascular disease.[53,54] The momentum to explore the use of technologies with telehealth more generally has only increased momentum due to the COVID-19 pandemic.[55] Technologies like those employed in this study may aid in minimizing the trade-off between patient comfort and signal integrity to allow for large datasets containing ambulatory EGG recordings and symptoms to be created in the comfort of one's home. This has the potential to propel machine learning and decision-support technologies and allow for physicians to improve their diagnosis and treatment of GI disorders.

4. Experimental Section

Electrodes Array Fabrication: A silicon wafer was cleaned with acetone, IPA, DI water, IPA followed by drying with N_2. It was then baked on a 180 °C hotplate to dry completely. The clean wafer was then spun-coated with polydimethylsiloxane at 4000 rpm which would act as a weakly adhering substrate for subsequent fabrication steps. Polyimide (HD Microsystems, Inc., Parlin, NJ) was spun-coated at 4000 rpm, followed by a soft bake of 110 °C for 1 min and 150 °C for 5 min, and a full hard in a N_2 rich environment oven at 300 °C. Polyimide acted as an insulator

for the following metal sensors and interconnects. Metallization of 10 nm chrome and 250 nm gold was then followed (Temescal BJD 1800 E-Beam Evaporator, Livermore, CA). Standard microfabrication procedures (photolithography and metal wet etching) were performed to define sensors and interconnects. Another layer of polyimide was then spun-coated, soft-baked, and hard-baked with the same parameters as above. The polyimide was then patterned via photolithography and reactive ion etching with O_2 plasma to define the insulator layer. 37.5 µm silver/silver chloride ink, 50% solid by volume (Creative Materials, Inc., Ayer, MA) was then deposited via screen printing (with 75 µm stainless steel stencil) onto the sensor areas. Water-soluble tape (3M, Inc., Saint Paul, MN) was then used to transfer-print the device from the silicon wafer to a polymethylmethacrylate-treated glass substrate (acted as a non-stick release layer) that was spun-coated at 3000 rpm with Ecoflex (Smooth On, Inc., Macungie, PA) which acted as a backbone silicone and Silbione RT Gel (Elkem, Inc., Brunswick, NJ) which acted as an adhesive silicone. A custom zero insertion force (ZIF) connector was then interfaced with the ten-electrode array using anisotropic tape which facilitated bonding (3M, Inc., Saint Paul, MN) by applying heat and pressure on the bonding sites.

Participants: Cutaneous recordings were performed on ten healthy subjects: age: 21 ± 2 years (range: 19–25 years); BMI: 22 ± 2 (range: 19–24).

Each subject was asked to fast prior to the start of the recording, for a duration of 90 min; 30 min preprandial and 60 min postprandial consumption. At the 30 min mark, a 250 kCal nutrient bar and 8 oz water was consumed by each participant.

Electrode Placement: A portable ultrasound was performed to guide placement of the multi-electrode array over the antrum. Ultrasound gel was used during ultrasound imaging of the stomach. Abdomen mode at 10 cm depth and 21–22 Hz frequency was used.

The device was then applied to the abdomen and the glass substrate was subsequently peeled off. The other end of the ZIF connector was attached to an adapter board (Adafruit Industries, Inc., New York, NY) which was then connected via jumper cables to a biopotential board (OpenBCI, Inc.) along with ground and reference electrodes (3M Red Dot, 3M, Inc., Saint Paul, MN).

Data Collection: After bonding with a custom connector, the device was then transferred to the abdomen where the stomach was located (verified using ultrasound via Butterfly IQ) and the glass substrate was subsequently peeled off (Figure 3c). The medical grade adhesive silicone enabled the device to attach conformally to the abdomen area. The other end of the ZIF connector was attached to an adapter board (Adafruit Industries, Inc., New York, NY) which was then connected via jumper cables to a Bluetooth biopotential board (OpenBCI, Inc.) along with ground and reference electrodes (3M Red Dot, 3M, Inc., Saint Paul, MN). Recording was performed and the data was streamed wirelessly to the OpenBCI GUI installed on a Microsoft Surface 3 computer (Microsoft, Inc., Redmond, WA). The choice of wireless biopotential data acquisition board was based on previously published findings that indicated adequate noise rejection and artifact rejection for ambulatory EGG monitoring using the same acquisition system.[17]

Data Processing: Signals from each electrode were recorded with the OpenBCI specifications pertaining to a gain of 24x, resulting in a scale factor of 0.02235 µV per count, and sampling rate of 250 Hz. After signals were down-sampling to 1 Hz, a finite impulse response filter was performed with pass-band frequencies between 0.015 and 0.15 Hz.[16] In order to eliminate movement related artifacts, an interference cancellation procedure was employed that used an interference cancellation procedure involving minimum mean squared estimation with locally estimated mean and variance statistics.[17] A short-time Fourier transform spectrogram with 75% overlap and Hamming window was implemented for each pair of measurement electrodes. SNR was defined as the average power (in dB) between 0.04 and 0.06 Hz subtracted from the average power in all other frequencies between 0.02 and 0.15 Hz.[17] The pair with highest SNR was identified and performed subsequent statistics based upon the waveform defined from the highest SNR pair. Baseline power was calculated as 3 dB above

the 98.5th percentile of the spectral power at frequencies above 0.07 Hz. Normalized EGG power was defined to be the power (in dB) calculated from the spectrogram between 0.03 and 0.07 Hz when it exceeded baseline power, and zero otherwise.

Human Experiment: Data collection was done as part of an ongoing study at the University of California, San Diego, whose institutional review board provided ethical approval (IRB number 141069 "A pilot trial to evaluate the utility of passive, skin-mounted electrodes to monitor the electrical activity of the human digestive system").

Conflict of Interest

The authors declare no conflict of interest.

Data Availability Statement

Research data are not shared.

[1] R. Brun, B. Kuo, *Ther. Adv. Gastroenterol.* **2010**, *3*, 3.
[2] A. Gikas, J. K. Triantafillidis, *Int. J. Gen. Med.* **2014**, *7*, 159.
[3] Z. S. Heetun, E. M. Quigley, *Parkinsonism Relat. Disord.* **2012**, *18*, 5.
[4] M. Horowitz, Y. C. Su, C. K. Rayner, K. L. Jones, *Can. J. Gastroenterol.* **2001**, *15*, 805.
[5] R. V. Corinaldesi, V. Stanghellini, C. Raiti, E. Rea, R. Salgemini, L. Barbara, *Gut* **1987**, *28*, 3.
[6] R. W. McCallum, O. Cynshi, Investigative Team, *Aliment. Pharmacol. Ther.* **2007**, *26*, 8.
[7] M. E. Barton, T. Otiker, L. V. Johnson, D. C. Robertson, R. L. Dobbins, H. P. Parkman, P. M. Hellstrom, J. F. Tack, B. Kuo, A. Hobson, G. E. Dukes, *Gastroenterology* **2014**, *146*, 5.
[8] T. L. Abell, A. Kedar, A. Stocker, K. Beatty, L. McElmurray, M. Hughes, H. Rashed, W. Kennedy, G. Wendelschafer-Crabb, X. Yang, M. Fraig, *Neurogastroenterol. Motil.* **2019**, *31*, 3.
[9] T. R. Angeli, L. K. Cheng, P. Du, T. H. H. Wang, C. E. Bernard, M. G. Vannucchi, M. S. Faussone-Pellegrini, C. Lahr, R. Vather, J. A. Windsor, G. Farrugia, T. L. Abell, G. O'Grady, *Gastroenterology* **2015**, *149*, 56.
[10] G. O'Grady, T. R. Angeli, P. Du, C. Lahr, W. J. Lammers, J. A. Windsor, T. L. Abell, G. Farrugia, A. J. Pullan, L. K. Cheng, *Gastroenterology* **2012**, *143*, 3.
[11] T. L. Abell, W. D. Johnson, A. Kedar, J. M. Runnels, J. Thompson, E. S. Weeks, A. Minocha, M. E. Griswold, *Gastrointest. Endoscopy* **2011**, *74*, 3.
[12] M. Elmasry, H. Hassan, H. Atassi, A. Stocker, L. McElmurray, K. Cooper, M. G. Hughes, C. Pinkston, T. Abell, *Gastroenterology* **2019**, *156*, 6.
[13] H. P. Parkman, W. L. Hasler, J. L. Barnett, E. Y. Eaker, *Neurogastroenterol. Motil.* **2003**, *15*, 2.
[14] *Handbook of Electrogastrography* (Eds: K. L. Koch, R. M. Stern), Oxford University Press, Oxford **2004**.
[15] S. Abid, G. Lindberg, *World J. Gastroenterol.* **2007**, *13*, 38.
[16] A. A. Gharibans, S. Kim, D. C. Kunkel, T. P. Coleman, *IEEE Trans. Biomed. Eng.* **2017**, *64*, 4.
[17] A. A. Gharibans, B. L. Smarr, D. C. Kunkel, L. J. Kriegsfeld, H. M. Mousa, T. P. Coleman, *Sci. Rep.* **2018**, *8*, 5019.
[18] A. A. Gharibans, T. P. Coleman, H. Mousa, D. C. Kunkel, *Clin. Gastroenterol. Hepatol.* **2019**, *17*, 13.
[19] L. A. Bradshaw, L. K. Cheng, E. Chung, C. B. Obioha, J. C. Erickson, B. L. Gorman, S. Somarajan, W. O. Richards, *Neurogastroenterol. Motil.* **2016**, *28*, 6.
[20] S. Somarajan, N. D. Muszynski, J. D. Olson, A. Comstock, A. C. Russell, L. S. Walker, S. A. Acra, L. A. Bradshaw, *Neurogastroenterol. Motil.* **2020**, e104035, https://doi.org/10.1111/nmo.14035.
[21] W. L. Hasler, *Gastroenterol. Clin.* **2020**, *49*, 519.
[22] D. H. Kim, N. Lu, R. Ma, Y. S. Kim, R. H. Kim, S. Wang, J. Wu, S. M. Won, A. Islam, K. J. Yu, T. Kim, R. Chowdhury, M. Ying, L. Xu, M. Li, H. Chung, H. Keum, M. McCormick, P. Liu, W. Zhang, F. G. Omenetto, Y. Huang, T. P. Coleman, J. A. Rogers, *Science* **2011**, *333*, 6044.
[23] H. U. Chung, B. H. Kim, J. Y. Lee, J. Lee, Z. Xie, E. M. Ibler, K. Lee, A. Banks, J. Y. Jeong, J. Kim, C. Ogle, D. Grande, Y. Yu, H. Jang, P. Assem, D. Ryu, J. W. Kwak, M. Namkoong, J. B. Park, Y. Lee, D. H. Kim, A. Ryu, J. Jeong, K. You, B. Ji, Z. Liu, Q. Huo, X. Feng, Y. Deng, Y. Xu, K. Jang, J. Kim, Y. Zhang, R. Ghaffari, C. M. Rand, M. Schau, A. Hamvas, D. E. Weese-Mayer, Y. Huang, S. M. Lee, C. H. Lee, N. R. Shanbhag, A. S. Paller, S. Xu, J. A. Rogers, *Science* **2019**, *363*, 6430.
[24] B. Xu, A. Akhtar, Y. Liu, H. Chen, W. Yeo, S. I. Park, B. Boyce, J. Kim, J. Yu, H. Lai, S. Jung, Y. Zhou, J. Kim, S. Cho, Y. Huang, T. Bretl, J. A. Rogers, *Adv. Mater.* **2016**, *28*, 22.
[25] P. Tallgren, S. Vanhatalo, K. Kaila, J. Voipio, *Clin. Neurophysiol.* **2005**, *116*, 4.
[26] A. Albulbul, *Bioengineering* **2016**, *3*, 3.
[27] P. Tallgren, S. Vanhatalo, K. Kaila, J. Voipio, *Clin. Neurophysiol.* **2005**, *116*, 4.
[28] Y. S. Kim, J. Lu, B. Shih, A. Gharibans, Z. Zou, K. Matsuno, R. Aguilera, Y. Han, A. Meek, J. Xiao, M. T. Tolley, T. P. Coleman, *Adv. Mater.* **2017**, *29*, 39.
[29] B. Tian, W. Yao, P. Zeng, X. Li, H. Wang, L. Liu, Y. Feng, C. Luo, W. Wu, *J. Mater. Chem.* **2019**, *7*, 809.
[30] R. Kumar, J. Shin, L. Yin, J. M. You, Y. S. Meng, J. Wang, *Adv. Energy Mater.* **2016**, *7*, 1602096.
[31] A. V. Mohan, N. Kim, Y. Gu, A. J. Bandodkar, J. M. You, R. Kumar, J. F. Kurniawan, S. Xu, J. Wang, *Adv. Mater. Technol.* **2017**, *2*, 4.
[32] A. J. Bandodkar, J. M. You, N. H. Kim, Y. Gu, R. Kumar, A. V. Mohan, J. F. Kurniawan, S. Imani, T. Nakagawa, B. Parish, M. Parthasarathy, *Energy Environ. Sci.* **2017**, *10*, 7.
[33] Normal Saline, https://www.ncbi.nlm.nih.gov/books/NBK545210/ (accessed: September 2020).
[34] M. Klett, J. A. Gilbert, K. Z. Pupek, S. E. Trask, D. P. Abraham, *J. Electrochem. Soc.* **2016**, *164*, A6095.

[35] A. Perlas, V. W. Chan, C. M. Lupu, N. Mitsakakis, A. Hanbidge, *Anesthesiology* **2009**, *111*, 82.

[36] J. Liang, J. Y. Cheung, J. D. Z. Chen, *Ann. Biomed. Eng.* **1997**, *25*, 850.

[37] X. Lin, D. Levanon, J. D. Z. Chen, *Dig. Dis. Sci.* **1998**, *43*, 1678.

[38] J. Chen, R. W. McCallum, *Med. Biol. Eng. Comput.* **1991**, *29*, 4.

[39] K. L. Koch, *Diabetes Technol. Ther.* **2001**, *3*, 51.

[40] S. Kim, C. J. Quinn, N. Kiyavash, T. P. Coleman, *Proc. IEEE* **2014**, *102*, 5.

[41] G. Schamberg, D. Ba, T. P. Coleman, *IEEE Trans. Signal Process.* **2018**, *66*, 12.

[42] S. E. Kim, M. K. Behr, D. Ba, E. N. Brown, *Proc. Natl. Acad. Sci. USA* **2018**, *115*, E5.

[43] K. J. Won, K. M. Sanders, S. M. Ward, *Proc. Natl. Acad. Sci. USA* **2005**, *102*, 41.

[44] J. Yin, J. D. Z. Chen, *J. Neurogastroenterol. Motil.* **2013**, *19*, 5.

[45] Y. Shimada, M. Watanabe, N. Shibahara, T. Kita, T. Itoh, K. Terasawa, *J. Gastroenterol.* **1998**, *33*, 3.

[46] A. Zhou, S. R. Santacruz, B. C. Johnson, G. Alexandrov, A. Moin, F. L. Burghardt, J. M. Rabaey, J. M. Carmena, R. Muller, *Nat. Biomed. Eng.* **2019**, *3*, 15.

[47] C. Kim, S. Joshi, H. Courellis, J. Wang, C. Miller, G. Cauwenberghs, *IEEE J. Solid-State Circuits* **2018**, *53*, 11.

[48] J. C. Erickson, J. A. Hayes, M. Bustamante, R. Joshi, A. Rwagaju, N. Paskaranandavadivel, T. R. Angeli, *Physiol. Meas.* **2018**, *39*, 3.

[49] P. Khader, T. Schicke, B. Röder, F. Rösler, *Int. J. Psychophysiol.* **2008**, *67*, 3.

[50] E. P. Stephen, G. C. Hotan, E. T. Pierce, P. G. Harrell, J. L. Walsh, E. N. Brown, P. L. Purdon, *Sci. Rep.* **2019**, *10*, 13701.

[51] D. J. Levinthal, P. L. Strick, *Proc. Natl. Acad. Sci. USA* **2020**, *117*, 3.

[52] D. Azzalini, I. Rebollo, C. Tallon-Baudry, *Trends Cognit. Sci.* **2019**, *23*, 6.

[53] P. J. Zimetbaum, M. E. Josephson, *Ann. Intern. Med.* **1999**, *130*, 10.

[54] M. P. Turakhia, D. D. Hoang, P. Zimetbaum, J. D. Miller, V. F. Froelicher, U. N. Kumar, X. Xu, F. Yang, P. A. Heidenreich, *Am. J. Cardiol.* **2013**, *112*, 4.

[55] S. Whitelaw, M. A. Mamas, E. Topol, H. G. Van Spall, *Lancet Digital Health* **2020**, *2*, E435.